Journal of the Indian Society of Remote Sensing
https://doi.org/10.1007/s12524-020-01301-6

RESEARCH ARTICLE

An Improved DDV Algorithm for the Retrieval of Aerosol Optical Depth From NOAA/AVHRR Data

Ruibo Li[1] · Lin Sun[1] · Huiyong Yu[1] · Jing Wei[2] · Xinpeng Tian[3]

Received: 9 October 2019 / Accepted: 25 December 2020

Abstract
Aerosol Optical Depth (AOD) is one of the important parameters to characterize the physical properties of the atmospheric aerosol, which is used to describe the extinction characteristics of the aerosol, and also to calculate the aerosol content, to assess the degree of air pollution and to study aerosol climate effect. To study the historical change of aerosol in long-time series, the advanced very high resolution radiometer (AVHRR) data earliest used for aerosol research was used in this study. Due to the lack of shortwave infrared (SWIR) (center at 2.13 μm) of the sensor, the relationship between the blue and red bands with SWIR cannot be provided, and the visible band used to calculate the normalized difference vegetation index (NDVI) contains the wavelength range of red and green, it is very difficult to calculate the accurate land surface reflectance (LSR). Therefore, based on the Dense Dark Vegetation algorithm (DDV), we propose to introduce mature MODIS vegetation index products (MYD13) to correct AVHRR NDVI, to support the estimation of AVHRR LSR, determine the relationship between corrected AVHRR NDVI and visible band LSR, and to carry out aerosol retrieval. The results show that about 63% of the data are within the error line, and there is a consistent distribution trend in the inter-comparison validation with MODIS aerosol products (MYD04).

Keywords AVHRR AOD · MODIS VI product · DDV algorithm

Introduction

Continuous research on the remote sensing method of the suspended particles in the atmosphere can promote the detection and exploration of particulate pollution (Pope III et al. 2002; Hoff and Christopher 2009). As one of the major components of air pollutants, aerosols partly offset the warming effect of greenhouse gases and mitigate global warming (McMurry 2000; Kulkarni et al. 2011). However, as a crucial parameter of the Earth-Atmosphere system, aerosols affect the global and local climate change through the direct and indirect radiative forcing: Firstly, when the radiation is scattered or absorbed by the aerosols, it reduces the radiation energy between the sun and earth's surface, and the absorption effect causes atmospheric circulation variation by altering the atmospheric heating rate (Sokolik and Toon 1996; Charlson et al. 1992). Secondly, aerosols can influence precipitation and visibility as cloud condensation, and the effect of particulate matter on cloud formation is mainly determined by the particle size and chemical composition of aerosol (Li et al. 2011; Várnai and Marshak 2018; Liu et al. 2019). In particular, fine aerosols, including PM10, PM2.5, and PM0.1 (Wei et al. 2019a; Wei et al. 2021a, b), may reach lung cells through human respiration, thus affecting human health (McGuinn et al. 2017; Hoff and Christopher 2009). Therefore, the monitoring of aerosol optical properties and spatio-temporal distribution characteristics is an important basis for an accurate evaluation of aerosol climate effects and effects on air quality (Al-Saadi et al. 2005).

✉ Lin Sun
sunlin@sdust.edu.cn

[1] College of Geodesy and Geomatics, Shandong University of Science and Technology, Qingdao 266590, Shandong, China

[2] Department of Atmospheric and Oceanic Science, Earth System Science Interdisciplinary Center, University of Maryland, College Park, MD, USA

[3] CAS Key Laboratory of Coastal Environmental Processes and Ecological Remediation, Yantai Institute of Coastal Zone Research, ChineseAcademy of Sciences, Yantai 264003, Shandong, China

Published online: 19 January 2021

Ground-based aerosol can provide detailed information about the optical and microphysical radiation properties of aerosol at the regional scale (Wang et al. 2015). From the characterizes of quick temporal and spatial variation of aerosol, the ground-based aerosol is much limited in revealing the spatial distribution and variation of aerosol. Meanwhile, satellite remote sensing techniques can realize a wide-scale, real-time, and synchronous aerosol observation, thereby providing an effective tool for aerosol research (Midhuna et al. 2017; Tian et al. 2018; Wei et al. 2019b; Tian et al. 2020).

Kaufman and Sendra (1988) proposed the DDV (Dense dark vegetation) algorithm for applying automatic atmospheric corrections to visible and near-infrared (NIR) satellite imagery. In the DDV algorithm, Kaufman et al. (1997a) regarded dense dark vegetation as a dark object and measured the land surface reflectance (LSR) of vegetated areas, such as pasture land and forests. In the pasture land, the range of reflectance is 0.025–0.04, and due to the shadows of tall vegetation, the reflectance can be decreased. The reflectance of forests is lower than that of pasture land, and the range is about 0.01–0.03. Considering the wide distribution of forests and their optical characteristics are rather stable, the dense dark vegetation was used to AOD retrieval and atmospheric correction. Future version of DDV algorithm have been applied to retrieve aerosol data over the land by using a moderate resolution imaging spectroradiometer (MODIS) (Zhang et al. 2019; Kaufman et al. 1997b; Levy et al. 2007). Compared with visible wavelength, the middle infrared (mid-IR) wavelength is less affected by aerosol, and the radiative effect factors of aerosol on the dark surfaces are more single than the brighter surfaces, dominated by the scattering effect. Therefore, Kaufman et al. (1997a) proposed the 3.8 μm and 2.13 μm reflectance relationship to reflectance in the visible bands. However, the reflectance of 3.8 μm has to be corrected for thermal emission and water vapor absorption. Therefore, these algorithms set the LSR to a fixed value and are either based on prior experience or the stable linear relationship between the LSR of blue and red bands with a shortwave infrared (SWIR) band.

The National Oceanic and Atmospheric Administration (NOAA) polar-orbiting meteorological series satellites launched in 1979, and the Advanced Very High Resolution Radiometer (AVHRR) aboard the NOAA can provide historical satellite data for nearly 40 years. Therefore, NOAA AVHRR data are crucial in aerosol research. AVHRR sensor is one of the earliest sensors used in marine aerosol research (Stowe et al. 1997, 2002; Husar et al. 1997; King et al. 1999). The sources of aerosol on the ocean are simple, and the aerosol model is fixed, in addition to extreme conditions (solar flare, etc.), the LSR on the ocean is very low in the blue, green, and NIR bands. Compared with marine aerosols, the terrestrial aerosols are affected by many factors, and LSR varies with time. Aerosol sources over land are complex, and there are obvious differences in the composition of different regions. Moreover, the land cover types are complicated and various, and the LSR of ground objects is different, and there are obvious differences in the composition of different regions. When the LSR is calculated, it is important to consider the contribution of the reflectance of the top of the atmosphere to different land cover types in aerosol retrieval.

Based on the DDV algorithm, Holben et al. (1992) retrieved AOD over land from AVHRR data with a visible band and revealed a close relationship between the dark targets and the normalized difference vegetation index (NDVI). In the retrieval experiments, the red and NIR bands in vegetated areas show obvious differences in their reflectance, the dark targets are determined via the spectral characteristics of vegetation in the visible and NIR bands, and the AOD over the Amazon forested region is retrieved considering the characteristics of the study area and under the assumption that the dark targets region has the LSR of 0.02. However, this method determines LSR based on experience, and the LSR does not take a fixed value because each region has varying surface characteristics. Therefore, many new algorithms for AOD retrieval have been proposed.

For instance, Takemata et al. (2006) fitted the LSR relations between the visible and third bands (3.55 μm–3.93 μm) by using 31 datasets. However, the radiance at 3.8 μm is affected both by thermal emission and by the reflected radiation from the solar. The variation of land surface temperature will have a great influence on the radiance, thereby increasing the uncertainty of the reflectance relationship between the two bands (Kerber and Schutt 1986). Mei et al. (2014) added the MODIS 2.13 μm band and VI to improve LSR estimation accuracy. Xue et al. (2017) established a statistical relationship between the LSRs of the visible and third bands combined with NDVI. These algorithms are improved by introducing VI, but the "apparent reflectance" instead of the "LSR" is used in the computational process. They do not consider the effects of atmospheric conditions on the VI. If the atmosphere is clear, then the atmosphere produces minimal influence on the VI, and such influence may be counteracted in the form of a "ratio" (Kaufman et al. 1992). However, an increase in the number of aerosol particles and water vapor in the atmosphere will either increase or decrease the apparent reflectance of the two bands, while the molecular scattering will increase such reflectance. In this case, when calculating VI, the "LSR" is not equal to the "apparent reflectance" (Goward et al. 1991). Hsu et al. (2017) described a new extension of the Deep Blue (DB)

algorithm to AVHRR over the land, and developed a modified NDVI database method to determine the LSR for AVHRR in the vegetated areas, this database was corrected with Rayleigh scattering and atmosphere (Sayer et al. 2017). However, this algorithm is greatly influenced by Aqua MODIS Collection 6 Deep Blue AOD product, to correct the background AOD for the NDVI database calculation.

In this paper, a new method for LSR estimation in AOD retrieval is proposed. Given the shortcoming of the AVHRR sensor, the process of LSR estimation in the DDV algorithm is improved. The MODIS VI product Collection 6 (MYD13 C6) is introduced into the estimation process to correct AHVRR NDVI, reduce the influence of the atmosphere, and the statistical relationship between NDVI and LSR is established by using the corrected AVHRR NDVI. Aerosol retrieval was performed using NOAA-19 AVHRR L1B data and uses the AOD measured on the ground (AErosol RObotic NETwork, AERONET) to validate the accuracy of the retrieved AOD and inter-comparison validation with MODIS aerosol products.

Materials and Methods

General Principle

The energy received by satellite is computed as follows:

$$\rho^*(\tau_\alpha, \mu_s, \mu_v, \phi) = \rho_0(\tau_\alpha, \mu_s, \mu_v, \phi) + \frac{\rho}{1 - \rho S(\tau_\alpha)} T(\tau_\alpha, \mu_s) T(\tau_\alpha, \mu_v) \quad (1)$$

where $\rho^*(\tau_\alpha, \mu_s, \mu_v, \phi)$ is the apparent reflectance at the TOA, $\rho_0(\tau_\alpha, \mu_s, \mu_v, \phi)$ is the path radiance coming from the Rayleigh scattering reflectance of atmospheric particles and the Mie scattering reflectance of aerosols, $T(\tau_\alpha, \mu_s)$ and $T(\tau_\alpha, \mu_v)$ are the downward and upward atmospheric transmissivities, and $S(\tau_\alpha)$ is the atmospheric hemispherical reflectance. μ_s and μ_v are the cosine values of θ_s (solar zenith angle) and θ_v (satellite zenith angle), ϕ is the relative azimuth angle between solar azimuth angle and satellite azimuth angle, and τ_α is the AOD.

Equation (1) shows that the difference between the apparent reflectance and LSR can be attributed to the contributions of substances (e.g., aerosols, clouds, and gases) to the apparent reflectance. However, the difficulty of aerosol retrieval in satellite remote sensing techniques is the decoupling of the earth-atmosphere system, it is crucial to separate the atmospheric effect from the surface effect and estimate the LSR. The spectral difference of vegetation at different bands (visible, NIR, SWIR bands) and atmospheric influence are the basis of AOD retrieval using the DDV algorithm (Kaufman and Sendra 1988; Kaufman et al. 1997a). However, the AVHRR sensor band does not apply to this algorithm, when the LSR needs to be determined by SWIR, because of its unique design. For AVHRR aerosol retrieval, the DDV algorithm mainly uses prior knowledge to determine the LSR. When the vegetation density is very dense, the reflectance is affected by shadows. However, the optical characteristics of dense vegetation are rather stable. Given that different vegetation types show minimal variances in their reflectance when the solar zenith angle is assumed constant (Kimes et al. 1986; Kaufman 1988). However, the dark targets are selected based on the empirical threshold of NDVI. Considering the limitations of the traditional AOD retrieval method, the AVHRR NDVI for selecting dark targets and calculating LSR can only be obtained based on the apparent reflectance after radiometric calibration, but the apparent reflectance includes atmospheric reflectance and LSR. Therefore, precisely calculating LSR is crucial in AOD retrieval. In this paper, AVHRR NDVI is calculated based on apparent reflectance and is corrected by using MYD13 NDVI. MYD13 is produced based on the MODIS LSR product, removes the influence of cloud, atmosphere, and nearby ground features. The AVHRR aerosol retrieval is realized by using the relationship between LSR in the visible band and NDVI.

Retrieval Model

The LSR of red and NIR bands can reduce the effects of clouds and atmospheric environments on the NDVI calculations. The analysis of the correlation between channel 1 and NDVI reveals the following linear relationship among the LSRs of the channel 1 with different vegetation coverages:

$$\rho^s_{red} = a_1 \times NDVI + b_1 \quad (2)$$

where ρ^s_{red} is the LSR of the channel 1, NDVI is the NDVI of densely vegetated areas, a_1 and b_1 are the correlation coefficients. NDVI is calculated as

$$NDVI = \frac{\rho^m_{NIR} - \rho^m_R}{\rho^m_{NIR} + \rho^m_R} \quad (3)$$

where ρ^m_{NIR} and ρ^m_R denote the reflectance of the NIR and red bands. The AVHRR data are resampled to a 1000 m resolution. Moreover, the effect of vegetation on AOD showed large spatial and temporal heterogeneity, the distribution and density of vegetation in various regions are different from each other. Thus, the AVHRR NDVI results need to be corrected (Mishra et al. 2018).

The same NDVI threshold is used to ignore the difference between the surface types, resulting in an inaccurate estimation of the LSR on the regional scale. Under a 1 km spatial resolution, the AVHRR data are divided into

10 km*10 km blocks, and the AVHRR NDVI is corrected by contrast stretching (Gillespie 1992; Yang 2006). To reduce the impact of calculation means and to improve the accuracy of the results, the AVHRR NDVI is corrected as follows (AVHRR $NDVI_{corr}$):

$$g(i,j) = \frac{b' - a'}{b - a}[f(i,j) - a] + a' \quad (4)$$

where $f(i,j)$ is the AVHRR NDVI, a' and b' are the minimum and maximum MYD13 NDVI values of vegetated areas, a and b are the minimum and maximum AVHRR NDVI values in the same vegetation areas, and $g(i,j)$ is the AVHRR $NDVI_{corr}$. MODIS VI products (MOD13 and MYD13) are developed based on existing VI and improves the AVHRR NDVI products (Nagol et al. 2014; Gitelson and Kaufman 1998). These products are calculated using the MODIS LSR products, avoid the water vapor absorption band at around 0.72 μm, and take some factors, such as atmosphere, angles, and leaf canopy background, into consideration. The 16-day synthesized global MYD13 A2 selects the optimal data through the maximum value composites and considers the influence of cloud and observation geometries, the marginal distortion is also corrected based on MODIS L1B data (Chen et al. 2011; Didan 2015). The MYD13 A2 with a spatial resolution of 1000 m (close to the resolution of AVHRR) is used to minimize the errors resulting from the joint usage of MODIS and AVHRR data. When determining a, b, a', and b', using MYD13 A2 to determine a proportion of dense vegetation pixels in the same area of AVHRR NDVI, the AVHRR NDVI is sorted via percentage matching to avoid direct pixel matching (Sun et al. 2010). Correcting AVHRR NDVI by using MYD13 NDVI avoids mutual spectral transformation and reduces the influence of the spectral differences among varying sensors on the accuracy of NDVI determination.

To accurately estimate the LSR in vegetated areas, the AERONET measurements, the AVHRR angle data, and the images after preprocessing are included in Eq. (1). The relationship between the AVHRR LSR of the visible band and $NDVI_{corr.}$ is then fitted based on the LSR estimations. The biggest difference between this method and the traditional algorithm is whether the LSR is a fixed value or not, and how to reduce the influence of the atmosphere in the calculation of AVHRR NDVI is considered. Using mature NDVI products to correct AVHRR NDVI can reduce the influence of atmospheric effects on NDVI and make NDVI more reliable. The correlation coefficient (R^2) between AVHRR $NDVI_{corr}$ and AVHRR LSR of the visible band is 0.5061:

$$\rho^s_{red} = -0.1415 \times NDVI_{corr} + 0.1548 \quad (5)$$

Based on the AVHRR LSR determination model (Eq. (5) and Fig. 1), and AOD retrieval is performed in mid-eastern America from June to October 2016.

Mid-eastern America (24°30′ to 46°49′N, 98°80′ to 72°20′W) is chosen as the study area, which is dominated by farmlands, forests, and grasslands, with high vegetation coverage (Fig. 2).

NOAA AVHRR Data

The NOAA satellite is equipped with the AVHRR, which is one of the earliest sensors applied in aerosol research. This radiometer has six spectral bands: 0.58–0.68 μm (channel 1), 0.72–1.0 μm (channel 2), 1.58–1.64 μm (channel 3A), 3.55–3.93 μm (channel 3B), 10.30–11.30 μm (channel 4), and 11.50–12.50 μm (channel 5), the spatial resolution in High Resolution Picture Transmission (HRPT) mode is 1.1 km by 1.1 km. The AVHRR has a wide swath of spatial coverage (2400 km), and observe the same position twice a day at 14:00 and 02:00 (ascending and descending). Because of the influence of the solar reflected signal, we can only use the daytime node here.

The NOAA-19 AVHRR L1B data are processed via radiometric calibration, geometric correction, and cloud detection. Details on the radiometric calibration method can be found in the NOAA KLM User Guide with NOAA-N, -N' Supplement (Goodrum et al. 2009). The calibration coefficients and observation geometries (e.g., solar zenith angle, view zenith angle, and relative azimuth angle) are obtained from the NOAA-19 AVHRR L1B data. The apparent reflectance of the visible and NIR bands as well as the brightness temperature of channel 4 and channel 5 are also obtained. Cloud detection is performed based on clouds in the AVHRR (CLAVR) algorithm, which is used to detect differences in the surface radiation characteristics (e.g., radiation emission and reflection, radiation wavelength, and spatial variation) and physical attributes of clouds and underlying surfaces (Stowe et al. 1991, 1999; Bulgin et al. 2018).

MODIS Product

The MODIS 16-days 1000 m VI product (MYD13A2 C6) supplies both NDVI and the Enhanced Vegetation Index (EVI), it is produced based on MODIS land surface reflectance product and corrected for atmospheric gasses and aerosols. The MODIS NDVI product was used in this study, after screening of data based on quality control and ancillary information, the two largest NDVI values for each pixel every 16 days were determined, finally, the NDVI value with the nearest to nadir view was selected (Gallo

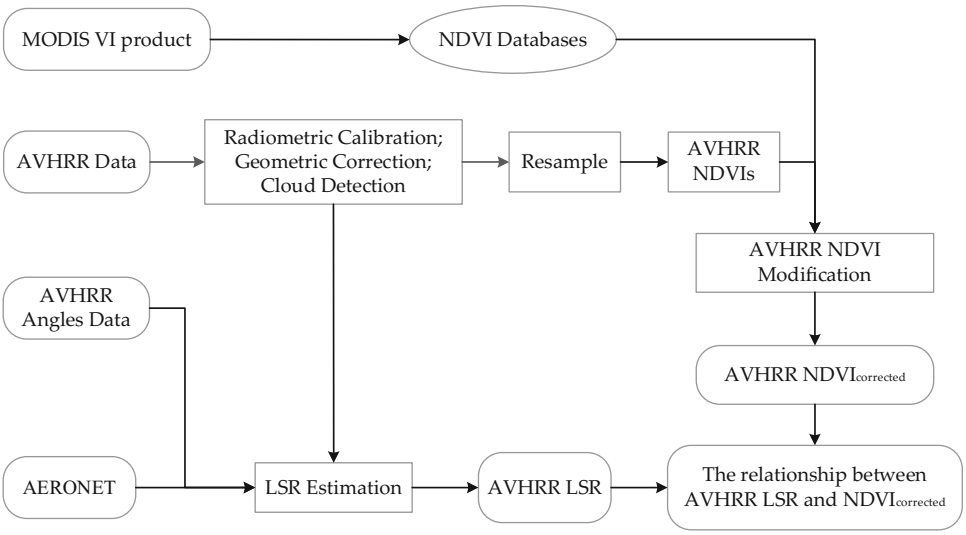

Fig. 1 Flow chart of the AVHRR LSR determination model

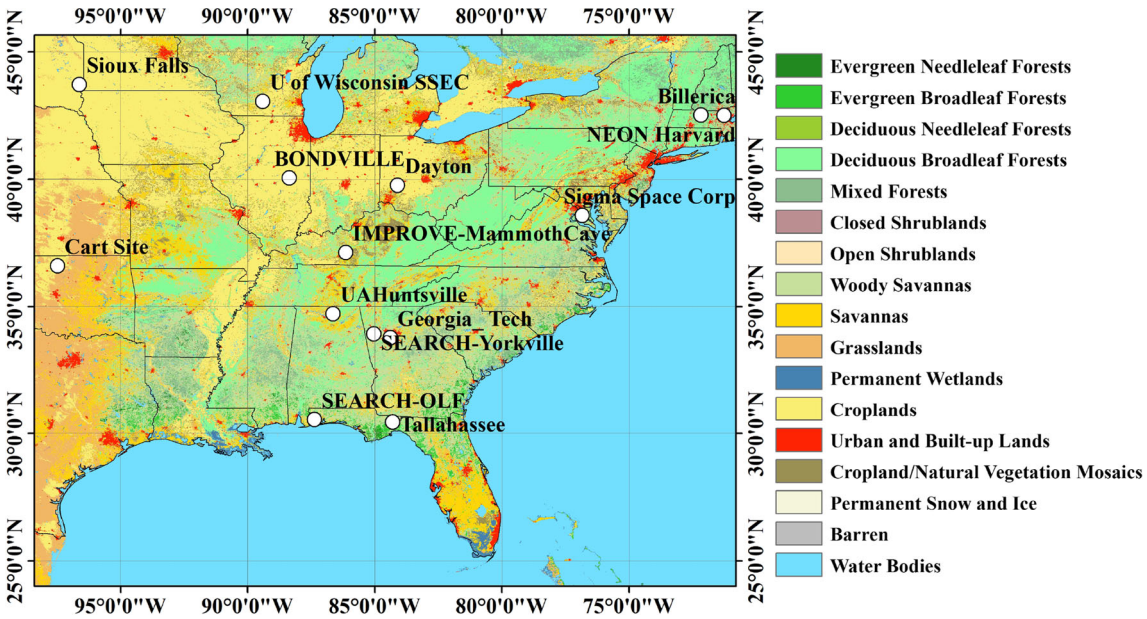

Fig. 2 The land cover type of study area and AERONET sites

et al. 2005). The MODIS NDVI product from June to October 2016 (summer and autumn) was selected to correct AVHRR NDVI, with a total of 10 images, Fig. 3 shows four NDVI images of the study area where the oceans and lakes are represented by the color blue and the NDVI is represented by the colors red and green with a range of −0.2–1. A positive NDVI indicates that the study area is covered with vegetation, while a negative or zero NDVI indicates that the study area is covered with clouds, water, snow, rocks, or bare soil. Most of the study area is covered with vegetation, and the coverage initially increases and then decreases.

The MODIS aerosol product (MOD04/MYD04) is currently available in three versions, namely, collection 6 (C6), collection 5.1 (C5.1), and collection 5 (C5). In C5, only the DDV algorithm is used for the land aerosol retrieval. Meanwhile, C6 and C5.1 are the improved versions of C5. The effects of cloud, scattering angle, and VI on AOD retrieval are taken into account in the DDV algorithm (Levy et al. 2007). For the bright areas (e.g., desert area, urban area, etc.) that cannot be retrieved by the DDV algorithm, the DB algorithm is introduced to extend the range of AOD retrieval (Hsu et al. 2019). Besides, two aerosol products (with 3 km and 10 km spatial resolutions) are available in C6. The MYD04 C6 (3 km) product was

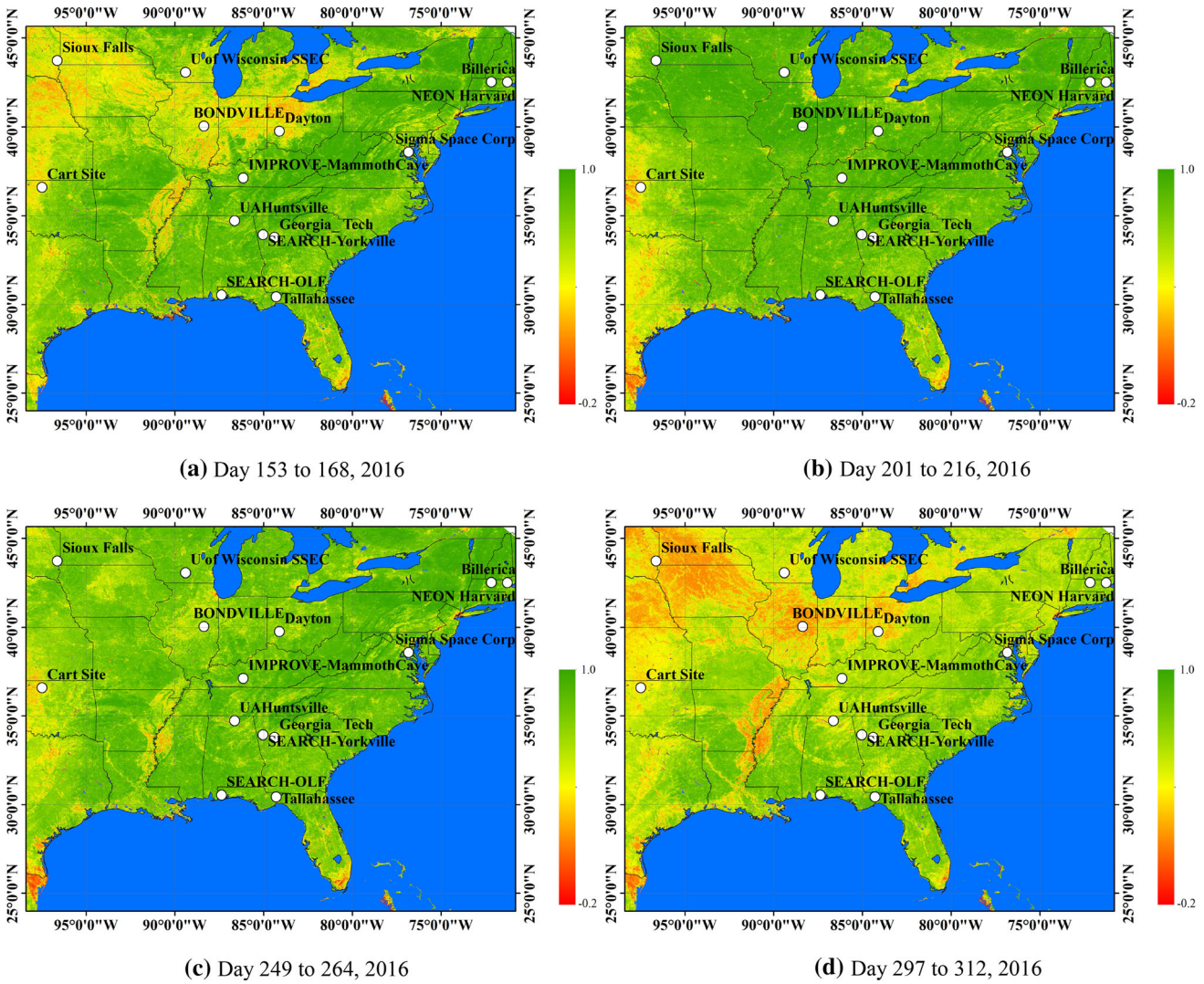

Fig. 3 Distribution of the MODIS VI product. **a** Day 153 to 168, 2016, **b** Day 201 to 216, 2016, **c** Day 249 to 264, 2016, **d** Day 297 to 312, 2016

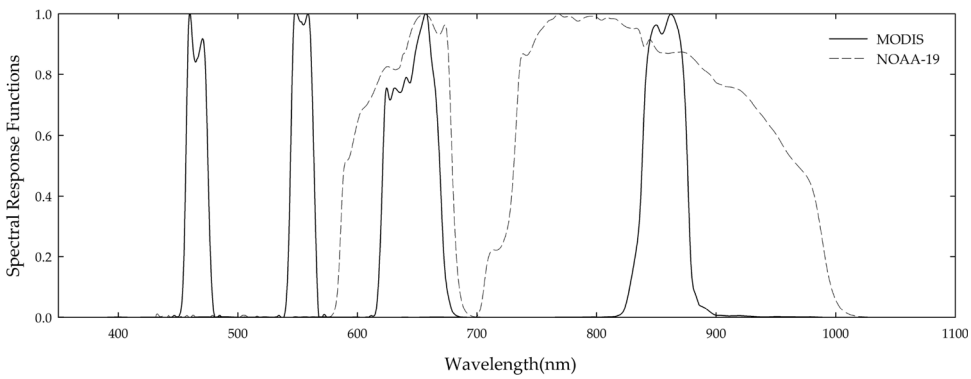

Fig. 4 Spectral response functions of NOAA-19 AVHRR and MODIS in the visible and NIR bands

selected as data in inter-comparison validation because it used traditional methods to reverse aerosols and was closest to the surface type in this study (Remer et al. 2013), and Fig. 4 shows the spectral response functions of the two sensors in the visible and NIR bands.

AERONET Ground-Measured Data

AERONET is a global network of ground-based sun/sky radiometers that mainly measures surface AOD, which is mainly used for evaluating the AOD retrieval results. This

tool provides long-term, continuous, and free aerosol datasets through network sharing. Aerosol data are acquired from the observation sites every 15 min. By providing ground monitoring data, AERONET reduces the influence of uncertain factors, such as atmosphere and cloud, and obtains a precision of about 0.01–0.02, which is three to five times larger than the precision achieved via satellite retrieval (Holben et al. 2001; Chin and Kahn 2009). AERONET also provides AOD values from three different levels (1.0, 1.5, and 2.0) and eight channels (340, 380, 440, 670, 870, 940, 1020, and 1640 nm). The levels 1.5 and 2.0 data are processed via cloud filtering and quality control (Giles et al. 2019; Wang et al. 2015). In this paper, levels 2.0 data are applied to 14 sites that are mainly distributed in vegetated areas (Fig. 2 and Table 1).

Results

Validation with the MODIS Aerosol Product

The MODIS aerosol product from the same region and with the same imaging time is used to compare with the AVHRR AOD. The same AERONET sites (levels 2.0) (Table 1) are used to verify daily AVHRR AOD and MYD04 AOD, and the results are shown in Fig. 5 (represented by three solid lines). It is found that the change of MYD04 AOD and AVHRR AOD is larger than that of AERONET AOD, the AOD varies from 0 to 0.4, and the consistency between MYD04 AOD and AERONET AOD is better than that of AVHRR AOD and AERONET AOD. However, the difference between the three data sets is almost less than 0.1. The reason may be that different observation modes between remote sensing and ground monitoring method, they are affected by different degrees of the atmosphere. Comparing the daily AVHRR AOD with MYD04 AOD (represented by a dotted line), the change of the difference between the two data is mainly related to the change of AVHRR AOD. One possible reason for this result is that this aerosol retrieval method of AVHRR is related to NDVI, and the change of NDVI will lead to different aerosol retrieval results. Another reason could be the limitation of AVHRR, such as the calibration method, cloud detection method. Because of the small number of spectral bands and a wide range of wavelengths in AVHRR, the result of cloud detection is not as good as that from MODIS.

In Fig. 6, the left panel represents the monthly AVHRR AOD, and the Right panel represents the collocated differences between the AVHRR AOD and MYD04 AOD over the same area from June to October. The difference maps (AVHRR AOD—MYD04 AOD) show that the AVHRR AOD is similar to the MYD04 AOD. By comparing the difference between the two data, the biases are generally between −0.1 and 0.1, and the influence of the cloud edge on AVHRR is reduced. These findings are similar to those obtained by previous studies (Xue et al. 2017; Sullivan et al. 2015). The result at 0.64 μm over many areas is lesser than 0.5. Besides, AVHRR AOD and MYD04 AOD apply different cloud detection algorithms, while the AVHRR data lack mature algorithms and products. MYD04 AOD has a higher retrieval accuracy and a more continuous spatial distribution than AVHRR AOD.

Validation with AERONET

To further evaluate the retrieval algorithm, 14 AERONET sites are selected for verification. Two types of data need to be matched to ensure the spectral, temporal, and spatial consistency of the verification data and AVHRR AOD.

Table 1 Information on the AERONET stations

Sites	Latitude (°N)	Longitude (°W)	Altitude (m)
Billerica	42.528	71.269	773
BONDVILLE	40.053	88.372	922
Cart Site	36.607	97.486	1020
Dayton	39.776	84.110	948
Georgia_Tech	33.780	84.400	986
IMPROVE-MammothCave	37.132	86.148	940
NEON Harvard	42.537	72.173	1060
SEARCH-OLF	30.550	87.375	752
SEARCH-Yorkville	33.928	85.046	1100
Sigma Space Corp	38.593	76.836	744
Sioux Falls	43.736	96.626	1190
Tallahassee	30.446	84.299	741
U of Wisconsin SSEC	43.072	89.411	973
UAHuntsville	34.725	86.645	906

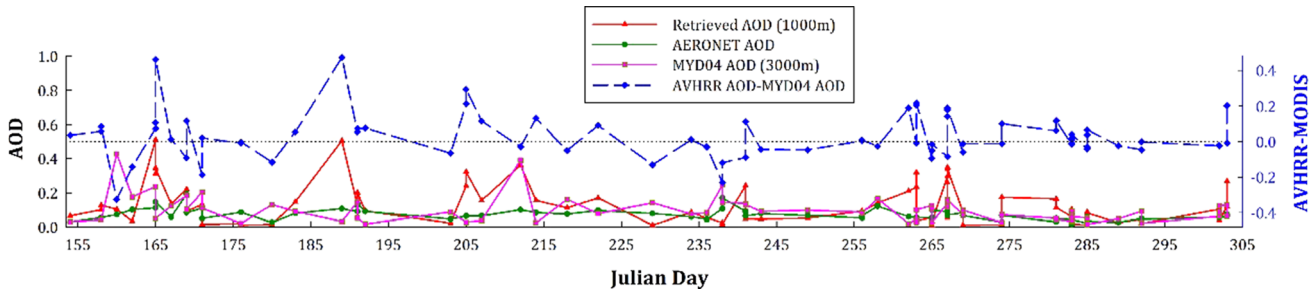

Fig. 5 Time series AOD from AVHRR, MYD04, and AERONET over six AERONET sites

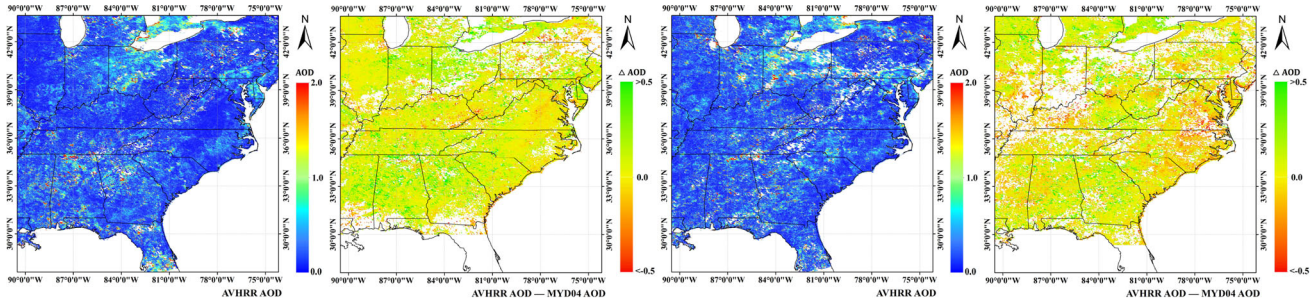

(a) Monthly average of 06/2016

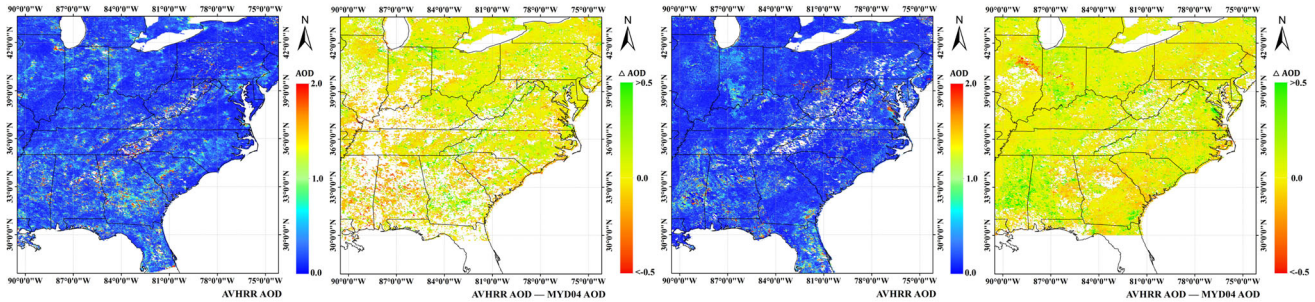

(b) Monthly average of 07/2016

(c) Monthly average of 08/2016

(d) Monthly average of 09/2016

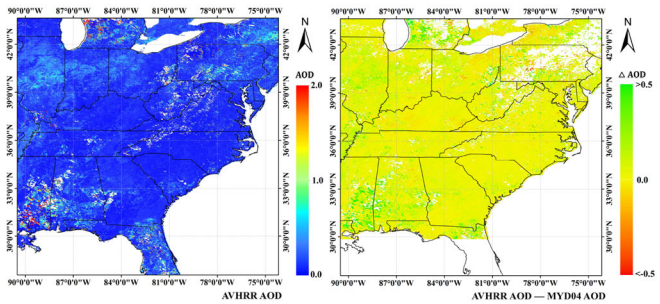

(e) Monthly average of 10/2016

Fig. 6 Monthly AOD from AVHRR AOD and the differences between the AVHRR AOD and MYD04 AOD: 1) AVHRR AOD and 2) AVHRR AOD—MYD04 AOD. **a** Monthly average of 06/2016, **b** Monthly average of 07/2016, **c** Monthly average of 08/2016, **d** Monthly average of 09/2016, **e** Monthly average of 10/2016

Given that aerosols are retrieved over the land at the visible band, the AERONET measurements at 675 nm are used for the verification. On the temporal scale, the AERONET measurements within ± 30 min of the satellite overpass time are used for the linear interpolation, and the satellite overpass time is set as the acquisition time (Sun et al. 2016). On the spatial scale, according to the cloud mask obtained by the CLAVR algorithm, the cloud cover within 10 km around the site is estimated and the clear pixels are selected for the verification.

$$EE = \pm(0.05 + 0.25\tau) \quad (6)$$

The retrieval results are evaluated according to the error criteria of AVHRR (Eq. (6)). Two types of data are compared based on the correlation coefficient (R) and root mean square error (RMSE). Figure 7 compares the regression analysis results for AVHRR AOD with the AERONET measurements at 14 sites, where the black dashed lines represent the error lines of AVHRR (Hsu et al. 2017; Sayer et al. 2017). Considering that the pixels involved in retrieval over the vegetation areas are clear sky pixels, AVHRR AOD and in situ AOD measurements are relatively small. There are 436 sets of data, and the correlation coefficient R is 0.2178. About 63% of the data are within the error line, with an RMSE of 0.13. Compared with the in situ AOD measurements, when the AVHRR AOD is greater than 0.2, there is an overestimation. The cause of overestimation may be cloud contamination, or inappropriate aerosol properties in the LUT because aerosols in mid-eastern America is dominated by fine mode aerosol with weak absorption (Li et al. 2013).

Discussion and Conclusion

Considering that the NDVI calculated by the apparent reflectance is used for the LSR estimation, which may cause larger errors in the AOD retrieval, therefore, the mature NDVI product was used to correct NDVI calculated by apparent reflectance in this study. The MYD13A2 NDVI product was selected, which the effects on the atmospheric gases, aerosol, thin cirrus clouds, water vapor, and ozone were considered more comprehensively, and the results after the atmosphere correction were more reliable. The AVHRR NDVI used in this paper was produced based on apparent reflectance, without atmosphere correction, aerosol particles usually cause an increase in the radiance in channel 1, and cause the mixed effect in channel 2, and water vapor reduces the apparent reflectance measured in channel 2, both effects reduce the vegetation index (Kaufman et al. 1992). This is also reflected in Table 2, the mean values of corrected AVHRR NDVI were greater than the mean values of uncorrected AVHRR NDVI. Therefore, it is very necessary to correct the NDVI without atmosphere correction.

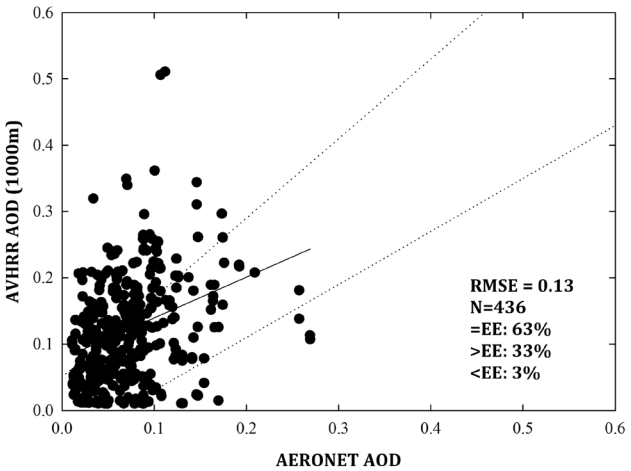

Fig. 7 Retrieval results of AERONET measurements and AVHRR AOD

To study the influence of uncorrected and corrected AVHRR NDVI on the accuracy of AOD retrieval, we also fitted the linear relationship between uncorrected AVHRR NDVIs and the LSRs of the channel 1 and used it for AOD retrieval, the correlation coefficient (R^2) between AVHRR NDVI and AVHRR LSR of the visible band was 0.3875, which was about 0.1 lower than the R^2 that corrected AVHRR NDVI. The monthly variations of the AOD retrieved using the uncorrected and corrected AVHRR NDVI, respectively, were calculated, Table 2 shows that the AOD retrieved using uncorrected AVHRR NDVIs were significantly overestimated, and the RMSEs were about 0.2, but the overestimated proportions of AOD retrieved using corrected AVHRR NDVIs were significantly reduced. It can be seen from Table 3 that the uncorrected AVHRR NDVIs were low, which lead to low LSRs and overestimation of AOD. The mature NDVI products were used to correct AVHRR NDVI, which can effectively improve the accuracy of AOD retrieval, but there was still an overestimation of 20%–40% and needs to be studied in the future.

In this paper, a method for LSR estimation of AVHRR sensors is proposed and applied to aerosol retrieval. This method mainly uses mature NDVI products, improves the AVHRR NDVI in LSR estimation, and applies it to mid-eastern America from June to October 2016. Based on the preprocessing and cloud detection of NOAA-19 AVHRR L1B data, aerosol retrieval is carried out. The key step is to use MYD13 NDVI, to improve AVHRR NDVI ($NDVI_{corr}$), and establish a statistical model between AVHRR LSR and $NDVI_{corr}$. The retrieval results obtained by the improved algorithm are validated. The results show that there is a good correlation with in situ AOD measurements and is consistent with the spatial distribution of MYD04 AOD products after monthly synthesis. Although this algorithm minimizes the disadvantages of using the DDV algorithm for AOD retrieval, future studies need to consider the following:

(1) When constructing the LSR dataset, the relationship between AVHRR NDVI and LSR is mainly considered. And this algorithm is mainly dependent on NDVI. Although NDVI has little change in a short

Table 2 The NDVI mean and stdev of uncorrected and corrected AVHRR NDVI

Time	AVHRR NDVI		AVHRR $NDVI_{corr}$		*N*
	NDVI mean	NDVI stdev	NDVI mean	NDVI stdev	
201,606	0.484	0.133	0.651	0.171	78
201,607	0.557	0.132	0.75	0.144	52
201,608	0.528	0.116	0.775	0.115	63
201,609	0.420	0.117	0.668	0.148	108
201,610	0.399	0.115	0.613	0.118	135

Table 3 The evaluation statistics of uncorrected and corrected AVHRR NDVI

Time	AVHRR NDVI				AVHRR $NDVI_{corr}$				*N*
	RMSE	Above EE (%)	Below EE (%)	Within EE (%)	RMSE	Above EE (%)	Below EE (%)	Within EE (%)	
201606	0.202	88.462	0.000	11.538	0.090	34.615	6.410	58.974	78
201607	0.208	84.615	1.923	13.462	0.095	23.077	5.769	71.154	52
201608	0.233	87.302	1.587	11.111	0.152	22.222	11.111	66.667	63
201609	0.183	87.037	0.000	12.963	0.097	41.667	0.000	58.333	108
201610	0.173	82.963	0.000	17.037	0.089	37.037	0.000	62.963	135

time on a regional scale, it is sensitive to the response of environmental changes over different regions. It has obvious temporal variation and spatial heterogeneity, leading to greater changes in AOD. Moreover, the AVHRR sensor has a large scanning angle and wide scene coverage. Therefore, the observation angle and other factors can bring some differences to the retrieval results.

(2) The requirements for effective cloud detection play a significant role in AOD retrieval. The observation cannot be effectively retrieved if contaminated by cloud or snow/ice. Besides, the reflection characteristics of typical surface types are analyzed, and the influence of LSR on aerosol retrieval is considered. The influence of other factors (e.g., aerosol type, seasonal conditions, etc.) needs to be studied further.

Retrieving long-term AOD over land from NOAA AVHRR data is of great significance in follow-up research. Future experiments need to consider more holistic data, such as aerosol properties and analyze the uncertainty of different aerosol and land cover types to improve the flexibility and precision of the algorithm.

Acknowledgements The authors thank the AERONET principal investigators and their staff for maintaining the sites and providing the data. We also thank the Goddard Space Flight Center (http://ladsweb.nascom.nasa.gov) for providing the MODIS data and the National Geophysical Data Center (https://www.class.ngdc.noaa.gov/saa/products/welcome) for providing the AVHRR data used in this paper. This research was funded by National Natural Science Foundation of China (No. 41771408) and the Shandong Provincial Natural Science Foundation, China (No. ZR2017MD001 and NO. ZR2020QD055).

Compliance with Ethical Standards

Conflict of interest The authors declare that they have no conflict of interest.

References

AlSaadi, J., Szykman, J. S., Pierce, R. B., Kittaka, C., Neil, D., Chu, D. A., et al. (2005). Improving national air quality forecasts with satellite aerosol observations. *Bulletin of the American Meteorological Society, 86*(9), 1249–1262. https://doi.org/10.1175/BAMS-86-9-1249.

Bulgin, C. E., Mittaz, J. P. D., Embury, O., Eastwood, S., & Merchant, C. J. (2018). Bayesian cloud detection for 37 years of advanced very high resolution radiometer (AVHRR) global area coverage (GAC) data. *Remote Sensing, 10*(1), 97. https://doi.org/10.3390/rs10010097.

Charlson, R. J., Schwartz, S. E., Hales, J. M., Cess, R. D., Coakley, J. A., Hansen, J. E., et al. (1992). Climate forcing by anthropogenic aerosols. *Science, 255*(5043), 423–430. https://doi.org/10.1126/science.255.5043.423.

Chen, Y., Long, B., Pan, X., Zhong, S., & Mo, W. (2011). Differences between MODIS NDVI and AVHRR NDVI in monitoring grasslands change. *Journal of Remote Sensing, 15*(4), 831–845.

Chin, M., & Kahn, R. (2009). Atmospheric Aerosol Properties and Climate Impacts. DIANE Publishing, p. 115.

Didan, K. MYD13A2 MODIS/Aqua Vegetation Indices 16-Day L3 Global 1km SIN Grid V006 (2015). NASA EOSDIS Land Processes DAAC. https://lpdaac.usgs.gov/documents/103/MOD13_User_Guide_V6.pdf. Accessed 2020–09–22.

Gallo, K., Ji, L., Reed, B., Eidenshink, J., & Dwyer, J. (2005). Multi-platform comparisons of MODIS and AVHRR normalized

difference vegetation index data. *Remote Sensing of Environment, 99*(3), 221–231. https://doi.org/10.1016/j.rse.2005.08.014.

Giles, D. M., Sinyuk, A., Sorokin, M. G., Schafer, J. S., Smirnov, A., Slutsker, I., et al. (2019). Advancements in the Aerosol Robotic Network (AERONET) Version 3 database – automated near-real-time quality control algorithm with improved cloud screening for Sun photometer aerosol optical depth (AOD) measurements. *Atmospheric Measurement Techniques, 12*(1), 169–209. https://doi.org/10.5194/amt-12-169-2019.

Gillespie, A. R. (1992). Enhancement of multispectral thermal infrared images: Decorrelation contrast stretching. *Remote Sensing of Environment, 42*(2), 147–155. https://doi.org/10.1016/0034-4257(92)90098-5.

Gitelson, A. A., & Kaufman, Y. J. (1998). MODIS NDVI optimization to fit the AVHRR data series—spectral considerations. *Remote Sensing of Environment, 66*(3), 343–350. https://doi.org/10.1016/S0034-4257(98)00065-0.

Goodrum, G., Kidwell, K. B., & Winston, W. (2009). NOAA KLM user's guide with NOAA-N,-N'supplement. Edition Jeffrey Robel. National Climatic Data Center, Asheville, Carolina, USA. Available at http://rain.atmos.colostate.edu/XCAL/docs/amsub/NOAA_KLM_Users_Guide.pdf.

Goward, S. N., Markham, B., Dye, D. G., Dulaney, W., & Yang, J. (1991). Normalized difference vegetation index measurements from the advanced very high resolution radiometer. *Remote Sensing of Environment, 35*(2), 257–277. https://doi.org/10.1016/0034-4257(91)90017-Z.

Hoff, R. M., & Christopher, S. A. (2009). Remote sensing of particulate pollution from space: Have we reached the promised land? *Journal of the Air and Waste Management Association, 59*(6), 645–675. https://doi.org/10.3155/1047-3289.59.6.645.

Holben, B. N., Tanré, D., Smirnov, A., Eck, T. F., Slutsker, I., Abuhassan, N., et al. (2001). An emerging ground-based aerosol climatology: Aerosol optical depth from AERONET. *Journal of Geophysical Research: Atmospheres, 106*(D11), 12067–12097. https://doi.org/10.1029/2001jd900014.

Holben, B. N., Vermote, E., Kaufman, Y. J., Tanre, D., & Kalb, V. (1992). Aerosol retrieval over land from AVHRR data-application for atmospheric correction. *IEEE Transactions on Geoscience and Remote Sensing, 30*(2), 212–222. https://doi.org/10.1109/36.134072.

Hsu, N. C., Lee, J., Sayer, A. M., Carletta, N., Chen, S. H., Tucker, C. J., et al. (2017). Retrieving near-global aerosol loading over land and ocean from AVHRR. *Journal of Geophysical Research: Atmospheres, 122*(18), 9968–9989. https://doi.org/10.1002/2017jd026932.

Hsu, N. C., Lee, J., Sayer, A. M., Kim, W., Bettenhausen, C., & Tsay, S. C. (2019). VIIRS deep blue aerosol products over land: extending the EOS long-term aerosol data records. *Journal of Geophysical Research: Atmospheres, 124*(7), 4026–4053. https://doi.org/10.1029/2018jd029688.

Husar, R. B., Prospero, J. M., & Stowe, L. L. (1997). Characterization of tropospheric aerosols over the oceans with the NOAA advanced very high resolution radiometer optical thickness operational product. *Journal of Geophysical Research: Atmospheres, 102*(D14), 16889–16909. https://doi.org/10.1029/96jd04009.

Kaufman, Y. J. (1988). Atmospheric effect on spectral signature-measurements and corrections. *IEEE Transactions on Geoscience and Remote Sensing, 26*(4), 441–450. https://doi.org/10.1109/36.3048.

Kaufman, Y. J., & Sendra, C. (1988). Algorithm for automatic atmospheric corrections to visible and near-IR satellite imagery. *International Journal of Remote Sensing, 9*(8), 1357–1381. https://doi.org/10.1080/01431168808954942.

Kaufman YJ, Tanré D, Holben BN, Markham BL, & Gitelson AA 1992 Atmospheric Effects on the NDVI–Strategies for its Removal. In Proceedings IGARSS '92 International Geoscience and Remote Sensing Symposium, 26–29 2, 1238–1241 https://doi.org/10.1109/IGARSS.1992.578402.

Kaufman, Y. J., Tanré, D., Remer, L. A., Vermote, E. F., Chu, A., & Holben, B. N. (1997a). Operational remote sensing of tropospheric aerosol over land from EOS moderate resolution imaging spectroradiometer. *Journal of Geophysical Research: Atmospheres, 102*(D14), 17051–17067. https://doi.org/10.1029/96jd03988.

Kaufman, Y. J., Wald, A. E., Remer, L. A., Gao, B., Li, R., & Flynn, L. (1997). The MODIS 2.1 μm channel-correlation with visible reflectance for use in remote sensing of aerosol. *IEEE Transactions on Geoscience and Remote Sensing, 35*(5), 1286–1298. https://doi.org/10.1109/36.628795.

Kerber, A. G., & Schutt, J. B. (1986). Utility of AVHRR channels 3 and 4 in land-cover mapping. *Photogrammetric Engineering and Remote Sensing*, *52*(1986), 1877–1883.

Kimes, D. S., Newcomb, W. W., Nelson, R. F., & Schutt, J. B. (1986). Directional reflectance distributions of a hardwood and pine forest canopy. *IEEE Transactions on Geoscience and Remote Sensing*, *24*(2), 281–293. https://doi.org/10.1109/TGRS.1986.289647.

King, M. D., Kaufman, Y. J., Tanré, D., & Nakajima, T. (1999). Remote sensing of tropospheric aerosols from space: Past, present, and future. *Bulletin of the American Meteorological Society, 80*(11), 2229–2260. https://doi.org/10.1175/1520-0477(1999)080%3c2229:RSOTAF%3e2.0.CO;2.

Kulkarni, P., Baron, P. A., & Willeke, K. (2011). *Aerosol measurement: principles, techniques, and applications*. New York: Wiley.

Levy, R. C., Remer, L. A., Mattoo, S., Vermote, E. F., & Kaufman, Y. J. (2007). Second-generation operational algorithm: Retrieval of aerosol properties over land from inversion of moderate resolution imaging spectroradiometer spectral reflectance. *Journal of Geophysical Research: Atmospheres*. https://doi.org/10.1029/2006jd007811.

Li, Y., Xue, Y., de Leeuw, G., Li, C., Yang, L., Hou, T., et al. (2013). Retrieval of aerosol optical depth and surface reflectance over land from NOAA AVHRR data. *Remote Sensing of Environment, 133,* 1–20. https://doi.org/10.1016/j.rse.2013.01.020.

Li, Z., Fan, J., Liu, Y., Rosenfeld, D., & Ding, Y. (2011). Long-term impacts of aerosols on the vertical development of clouds and precipitation. *Nature Geoscience, 4*(12), 888–894. https://doi.org/10.1038/ngeo1313.

Liu, D., Zhao, T., Boiyo, R., Chen, S., Lu, Z., Wu, Y., et al. (2019). Vertical structures of dust aerosols over East Asia Based on CALIPSO retrievals. *Remote Sensing, 11*(6), 701. https://doi.org/10.3390/rs11060701.

McGuinn, L. A., Ward-Caviness, C., Neas, L. M., Schneider, A., Di, Q., Chudnovsky, A., et al. (2017). Fine particulate matter and cardiovascular disease: Comparison of assessment methods for long-term exposure. *Environmental Research, 159,* 16–23. https://doi.org/10.1016/j.envres.2017.07.041.

McMurry, P. H. (2000). A review of atmospheric aerosol measurements. *Atmospheric Environment, 34*(12), 1959–1999. https://doi.org/10.1016/S1352-2310(99)00455-0.

Mei, L. L., Xue, Y., Kokhanovsky, A. A., von Hoyningen-Huene, W., de Leeuw, G., & Burrows, J. P. (2014). Retrieval of aerosol optical depth over land surfaces from AVHRR data. *Atmospheric Measurement Techniques, 7*(8), 2411–2420. https://doi.org/10.5194/amt-7-2411-2014.

Midhuna, T. M., Gharai, B., Jose, S., Rao, N., & P. V. . (2017). Study on regional variations of aerosol loading using long term satellite data over Indian region. *Journal of the Indian Society of Remote*

Sensing, 45(4), 685–697. https://doi.org/10.1007/s12524-016-0622-1.

Mishra, A. K., Banerjee, T., Kant, Y., Shaik, D. S., & Singh, A. K. (2018). Retrieval of aerosol optical depth over land at 0.490 μm from oceansat-2 data. *Journal of the Indian Society of Remote Sensing, 46*(5), 761–769. https://doi.org/10.1007/s12524-017-0715-5.

Nagol, J. R., Vermote, E. F., & Prince, S. D. (2014). Quantification of impact of orbital drift on inter-annual trends in AVHRR NDVI data. *Remote Sensing, 6*(7), 6680–6687. https://doi.org/10.3390/rs6076680.

Pope, C. A., III., Burnett, R. T., Thun, M. J., Calle, E. E., Krewski, D., Ito, K., et al. (2002). Lung cancer, cardiopulmonary mortality, and long-term exposure to fine particulate air pollution. *JAMA, 287*(9), 1132–1141. https://doi.org/10.1001/jama.287.9.1132.

Remer, L. A., Mattoo, S., Levy, R. C., & Munchak, L. A. (2013). MODIS 3 km aerosol product: Algorithm and global perspective. *Atmospheric Measurement Techniques, 6*(7), 1829–1844. https://doi.org/10.5194/amt-6-1829-2013.

Sayer, A. M., Hsu, N. C., Lee, J., Carletta, N., Chen, S. H., & Smirnov, A. (2017). Evaluation of NASA Deep Blue/SOAR aerosol retrieval algorithms applied to AVHRR measurements. *Journal of Geophysical Research: Atmospheres, 122*(18), 9945–9967. https://doi.org/10.1002/2017jd026934.

Sokolik, I. N., & Toon, O. B. (1996). Direct radiative forcing by airborne mineral aerosols. *Journal of Aerosol Science, 27,* S11. https://doi.org/10.1016/0021-8502(96)00078-x.

Stowe, L. L., Davis, P. A., & McClain, E. P. (1999). Scientific basis and initial evaluation of the CLAVR-1 global clear/cloud classification algorithm for the advanced very high resolution radiometer. *Journal of Atmospheric and Oceanic Technology, 16*(6), 656–681. https://doi.org/10.1175/1520-0426(1999)016%3c0656:SBAIEO%3e2.0.CO;2.

Stowe, L. L., Ignatov, A. M., & Singh, R. R. (1997). Development, validation, and potential enhancements to the second-generation operational aerosol product at the national environmental satellite, data, and information service of the national oceanic and atmospheric administration. *Journal of Geophysical Research: Atmospheres, 102*(D14), 16923–16934. https://doi.org/10.1029/96jd02132.

Stowe, L. L., Jacobowitz, H., Ohring, G., Knapp, K. R., & Nalli, N. R. (2002). The advanced very high resolution radiometer (AVHRR) pathfinder atmosphere (PATMOS) Climate dataset: Initial analyses and evaluations. *Journal of Climate, 15*(11), 1243–1260. https://doi.org/10.1175/1520-0442(2002)015%3c1243:TAVHRR%3e2.0.CO;2.

Stowe, L. L., McClain, E. P., Carey, R., Pellegrino, P., Gutman, G. G., Davis, P., et al. (1991). Global distribution of cloud cover derived from NOAA/AVHRR operational satellite data. *Advances in Space Research, 11*(3), 51–54. https://doi.org/10.1016/0273-1177(91)90402-6.

Sullivan, R. C., Levy, R. C., & Pryor, S. C. (2015). Spatiotemporal coherence of mean and extreme aerosol particle events over eastern North America as observed from satellite. *Atmospheric Environment, 112,* 126–135. https://doi.org/10.1016/j.atmosenv.2015.04.026.

Sun, L., Sun, C., Liu, Q., & Zhong, B. (2010). Aerosol optical depth retrieval by HJ-1/CCD supported by MODIS surface reflectance data. *Science China Earth Sciences, 53*(1), 74–80. https://doi.org/10.1007/s11430-010-4134-5.

Sun, L., Yu, H., Fu, Q., Wang, J., Tian, X., & Mi, X. (2016). Aerosol optical depth retrieval and atmospheric correction application for GF1 PMS supported by land surface reflectance data. *Journal of Remote Sensing, 20,* 216–228.

Takemata, K., Fukui, H., & Kawata, Y. (2006). Retrieval of aerosol optical thickness over land using NOAA/AVHRR data. *Advances in Space Research, 38*(10), 2208–2211. https://doi.org/10.1016/j.asr.2006.03.042.

Tian, X., Liu, S., Sun, L., & Liu, Q. (2018). Retrieval of Aerosol optical depth in the arid or semiarid region of Northern Xinjiang China. *Remote Sensing, 10*(2), 197. https://doi.org/10.3390/rs10020197.

Tian, X., Liu, Q., Gao, Z., Wang, Y., Li, X., & Wei, J. (2020). Improving MODIS aerosol estimates over land with the surface BRDF reflectances using the 3-D discrete cosine transform and RossThick-LiSparse models. *IEEE Transactions on Geoscience and Remote Sensing*. https://doi.org/10.1109/TGRS.2020.3048109.

Várnai, T., & Marshak, A. (2018). Satellite observations of cloud-related variations in aerosol properties. *Atmosphere, 9*(11), 430. https://doi.org/10.3390/atmos9110430.

Wang, J., Zhu, C., Zhu, Y., & Chen, S. (2015). Characterization of aerosol properties in beijing from long-term AERONET monitoring (2003–2012). *Journal of the Indian Society of Remote Sensing, 43*(4), 825–839. https://doi.org/10.1007/s12524-014-0441-1.

Wei, J., Li, Z., Guo, J., Sun, L., Huang, W., Xue, W., et al. (2019a). Satellite-Derived 1-km-Resolution PM1 Concentrations from 2014 to 2018 across China. *Environmental Science & Technology*, *53*(22), 13265–13274. https://doi.org/10.1021/acs.est.9b03258.

Wei, J., Peng, Y., Guo, J., & Sun, L. (2019b). Performance of MODIS Collection 6.1 Level 3 aerosol products in spatial-temporal variations over land. *Atmospheric Environment*, *206*, 30–44. https://doi.org/10.1016/j.atmosenv.2019.03.001.

Wei, J., Li, Z., Lyapustin, A., Sun, L., Peng, Y., Xue, W., et al. (2021a). Reconstructing 1-km-resolution high-quality PM2.5 data records from 2000 to 2018 in China: spatiotemporal variations and policy implications. *Remote Sensing of Environment*, *252*, 112136. https://doi.org/10.1016/j.rse.2020.112136.

Wei, J., Li, Z., Xue, W., Sun, L., Fan, T., Liu, L., et al. (2021b). The ChinaHighPM10 dataset: generation, validation, and spatiotemporal variations from 2015 to 2019 across China. *Environment International*, *146*, 106290. https://doi.org/10.1016/j.envint.2020.106290.

Xue, Y., He, X., de Leeuw, G., Mei, L., Che, Y., Rippin, W., et al. (2017). Long-time series aerosol optical depth retrieval from AVHRR data over land in North China and Central Europe. *Remote Sensing of Environment, 198,* 471–489. https://doi.org/10.1016/j.rse.2017.06.036.

Yang, C.-C. (2006). Image enhancement by modified contrast-stretching manipulation. *Optics and Laser Technology, 38*(3), 196–201. https://doi.org/10.1016/j.optlastec.2004.11.009.

Zhang, L., Zhang, M., & Yao, Y. (2019). Multi-Time Scale Analysis of Regional Aerosol Optical Depth Changes in National-Level Urban Agglomerations in China Using Modis Collection 61 Datasets from 2001 to 2017. *Remote Sensing, 11*(2), 201. https://doi.org/10.3390/rs11020201.